

Article

Up-Conversion Photoluminescence in Thulia and Ytterbia Co-Doped Ytria-Stabilized Zirconia Single Crystals

Danni Huang¹, Tong Xiao¹, Beibei Fu¹, Shoulei Xu^{1,*}, Yuyang Huang^{1,*}, Wen Deng¹ and Zhukun Zhou^{2,*}¹ School of Physical Science and Technology, Guangxi University, 100 East Daxue Road, Nanning 530004, China² School of Mechanical Engineering, Guangxi University, 100 East Daxue Road, Nanning 530004, China

* Correspondence: xsl@gxu.edu.cn (S.X.); panyy@gxu.edu.cn (Y.H.); zhukunzhou@gxu.edu.cn (Z.Z.);

Tel.: +86-771-3232666 (S.X.)

Abstract: ZrO₂ is an attractive host matrix for luminescence material because of its excellent physical properties, such as low phonon energy and wide band gap. In this work, the highly transparent Tm₂O₃ and Yb₂O₃ co-doped yttria stabilized zirconia (YSZ) (abbreviated as Yb/Tm: YSZ) single crystals were grown by the optical floating zone method. The Yb/Tm: YSZ samples were stabilized in the cubic phase at room temperature when Yb³⁺ and Tm³⁺ replaced Y³⁺. The influence of Yb³⁺ co-doping on the up-conversion luminescence properties of the crystals was systematically studied. A total of 0.5 mol% Tm₂O₃ and 2.0 mol% Yb₂O₃ co-activated YSZ single crystal (abbreviated as 2.0Yb/Tm: YSZ) has the maximum luminous intensity. There were seven absorption peaks located at around 358, 460, 679, 783.3, 850–1000, 1200, and 1721.5 nm that were observed in the absorption spectrum of the 2.0Yb/Tm: YSZ single crystal. There were three up-conversion peaks at around 488, 658 and 800 nm that were observed when the Yb/Tm: YSZ samples were excited at 980 nm. The fluorescence lifetime of Tm³⁺ for the ¹G₄→³H₆ transition of the 2.0Yb/Tm: YSZ sample is 7.716 ms as excited with a 980 nm laser. In addition, the oscillator strength parameters Ω_{λ} ($\lambda = 2, 4$ and 6) of this sample were derived by the Judd–Ofelt theory to evaluate the laser performance of the host materials. The ratio Ω_4/Ω_6 of this sample is 0.80, implying its excellent laser output. Therefore, the 2.0Yb/Tm: YSZ single crystal is a considerable potential material for laser and luminescence applications.



Citation: Huang, D.; Xiao, T.; Fu, B.; Xu, S.; Huang, Y.; Deng, W.; Zhou, Z. Up-Conversion Photoluminescence in Thulia and Ytterbia Co-Doped Ytria-Stabilized Zirconia Single Crystals. *Crystals* **2023**, *13*, 460.

<https://doi.org/10.3390/cryst13030460>

Academic Editor: Maria Milanova

Received: 24 February 2023

Revised: 3 March 2023

Accepted: 4 March 2023

Published: 7 March 2023



Copyright: © 2023 by the authors. Licensee MDPI, Basel, Switzerland. This article is an open access article distributed under the terms and conditions of the Creative Commons Attribution (CC BY) license (<https://creativecommons.org/licenses/by/4.0/>).

Keywords: YSZ single crystal; Yb³⁺ and Tm³⁺ co-activated; optical floating zone method; up-conversion luminescence; Judd–Ofelt theory

1. Introduction

Rare earth ions activated up-conversion luminescence material can convert near-infrared light into visible light by absorbing two or more low-energy photons and emitting one high-energy photon. This phenomenon violates the Stokes law, called the anti-Stokes luminescence or the up-conversion luminescence [1]. As they can emit short wavelength (high energy) light under the excitation of long wavelength (low energy) light source, the up-conversion luminescent materials have attracted great attention in the field of the infrared anti-counterfeiting, the anti-stokes cold light refrigeration, the up-conversion laser, the up-conversion 3D display, the sensing, and the medical applications [2–7].

As the emitted photon energy is greater than that of the excited ones, the energy levels between the activator and the sensitizer have to be very close to realize the continuous absorption of photons and energy transfer in the up-conversion luminescence process. Among the trivalent rare earth ions, Tm³⁺ is an important up-conversion luminescence activator. It has a ladder-like schema of energy level, and its ¹D₂→³F₄ and ¹G₄→³H₆ transition wavelengths are around 450 and 480 nm, respectively. The blue up-conversion luminescence process of Tm³⁺ can be excited under the pumping at 650, 800, and 980 nm. Tm³⁺ has been extensively studied due to its suitability for commercial InGaAs (940–990 nm) laser diode pumping. Yb³⁺ has the electronic configuration of 4f¹³, and its energy state

structure only contains one excited state (${}^2F_{5/2}$), which is slightly higher than the metastable excited state of Tm^{3+} (3H_5). Besides, Yb^{3+} has a strong absorption cross-section at 980 nm. The effective energy transfer can occur between Yb^{3+} and Tm^{3+} , achieving efficient up-conversion luminescence. The co-doping of Yb^{3+} and Tm^{3+} can substantially improve the up-conversion luminescence efficiency [8–12], which was widely adopted in investigating and utilizing light radiation.

The efficiency of up-conversion luminescence material depends not only on the characteristics of rare earth ions, but also on the host material [13–16]. Seeking appropriate host materials to achieve high efficiency, high sensitivity, and a stable up-conversion luminescence laser remains a challenge. Among various inorganic host materials, fluorides were widely studied because of their lower phonon energy and higher up-conversion emission efficiency. However, their chemical and thermal instability limits the potential applications in different environments. Besides, the sensitivities of present optical thermal sensors decline rapidly with increasing temperature. Oxide materials have attracted extensive attention because of their stable physical and chemical properties, such as good thermal stability, oxidation resistance, high mechanical strength, and being green and pollution-free.

Among many oxides, zirconia (ZrO_2) is proven to be an excellent matrix material for the trivalent lanthanide ions doping due to its low phonon energy (470 cm^{-1}) [8], wide band gap (5.0 eV) [9], high density, low thermal expansion, and large chemical stability. However, the ZrO_2 has three phases, including monoclinic (lower than $1170\text{ }^\circ\text{C}$), tetragonal ($1170\text{ }^\circ\text{C}$ – $2370\text{ }^\circ\text{C}$), and cubic (larger than $2370\text{ }^\circ\text{C}$) [9]. The phase transformation of ZrO_2 often comes with a volume change, leading to cracking. It is necessary to keep ZrO_2 stable in the cubic phase. One of the important ways is adding the stabilizers to ZrO_2 to form a stable solid solution. The more common way is adding 8 mol% Y_2O_3 to ZrO_2 to form the yttria zirconia solid (YSZ) solution, which has a cubic structure from room temperature to the melting point.

It is difficult to prepare high quality YSZ single crystal by conventional methods due to its high melting point ($2700\text{ }^\circ\text{C}$). The optical floating zone technology can concentrate the light at the same point to increase the heating temperature to $3000\text{ }^\circ\text{C}$. Also, it can be used to grow metal oxide single crystals with a high melting point as no crucible is needed in the growth process. Our research group has successfully grown $Y_3Al_5O_{12}$ [17–20] and ruby [20,21] single crystals by this method. Therefore, in this work, the YSZ single crystals co-activated by various concentrations of Yb^{3+} and Tm^{3+} were grown by the optical floating zone technology. The structure and up-luminescence properties of the samples were characterized. Moreover, we utilized the Judd–Ofelt theory to analyze the spectral parameters of Tm^{3+} and Yb^{3+} in the samples.

2. Materials and Methods

2.1. Crystal Growth

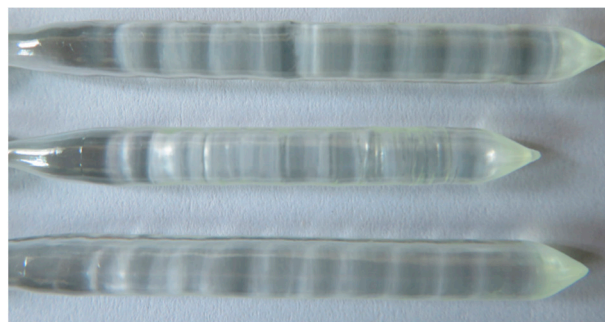
A series of polycrystalline ceramic rods were prepared through a solid-state reaction process before the single crystal growth. The oxides ZrO_2 (99.99%), Y_2O_3 (99.99%), Tm_2O_3 (99.99%), and Yb_2O_3 (99.99%) powders (Aladdin, Shanghai, China) were employed as raw materials. The appropriate amounts of powders were weighed at specified mole ratios (as seen in Table 1) and mixed homogeneously by a magnetic stirrer for 24 h. Then, each mixture was oven-dried at $85\text{ }^\circ\text{C}$ for 24 h and grounded in an agate mortar for 0.5 h. The prepared powder was packed in a long rubber balloon, vacuumed, sealed, and isostatically pressed under a pressure of 68 MPa to obtain the feed and seed rods. The obtained rods were sintered at $1550\text{ }^\circ\text{C}$ for 10 h in the air to be compact and uniform polycrystalline ceramic rods.

Table 1. Chemical compositions of Tm_2O_3 and Yb_2O_3 co-activated YSZ single crystals.

Samples	Composition (mol%)		
	YSZ	Tm_2O_3	Yb_2O_3
1.0Yb/Tm: YSZ	98.5	0.5	1.0
2.0Yb/Tm: YSZ	97.5	0.5	2.0
3.0Yb/Tm: YSZ	96.5	0.5	3.0
4.0Yb/Tm: YSZ	95.5	0.5	4.0
5.0Yb/Tm: YSZ	94.5	0.5	5.0

Single crystals of Tm_2O_3 and Yb_2O_3 co-doped YSZ were grown using an optical floating zone furnace (FZ-T-12000-X-VII-VPO-GU-PC, Crystal Systems Co., Yamanashi, Japan). During growth, a counter-rotated seed of 10 rpm of the seed and feed rods, a flow rate of 4 L/min of air was maintained, and the crystal growth rate was about 5 mm/h.

The as-grown Yb/Tm: YSZ single crystals were colorless and about 5×80 mm in size, as shown in Figure 1. The crystals had a smooth surface and were free from cracks. The chips of about 1.0 mm in thickness were cut from the Yb/Tm: YSZ crystal rods and then double-sided polished.

**Figure 1.** Yb/Tm:YSZ single crystal rods grown by the optical floating zone method.

2.2. Characterization

The X-ray diffraction (XRD) patterns were collected by a diffractometer (DX-2700, Haoyuan, Dangdong, China) using $\text{Cu-K}\alpha$ ($\lambda = 1.5406 \text{ \AA}$) radiation in the 2θ range of 20° – 80° with a step of 0.02° . The existing phases of as-prepared crystal chips were investigated also by Raman scattering. The Raman spectra in the wavenumber range of 150 – 950 cm^{-1} were obtained by a confocal Raman spectrometer (inVia Reflex, Renishaw, London, UK) with the laser excitation at 532 nm.

The absorption spectra of crystal chips were collected on a UV-Visible-NIR spectrophotometer (UV-3600, Shimadzu, Kyoto, Japan) with a resolution of 1 nm. The steady emission spectra were measured by a photoluminescence (PL) spectrometer (ZLF325, Zolix Instruments Co., Ltd, Beijing, China) with a 980 nm laser diode as an excitation source. Fluorescence decay curves were recorded with a fluorescence spectrometer (FLS920, Edinburgh Instruments, Edinburgh, UK) excited with a 980 nm laser as the excitation light.

3. Results and Discussion

3.1. Structure Analysis

The as-grown Yb/Tm: YSZ single crystals were crushed and ground into a powder to obtain detailed structure information. The XRD patterns of Yb/Tm: YSZ powders are shown in Figure 2a. For all the samples, six peaks were detected. It is impossible to identify the cubic and the tetragonal ZrO_2 as they share very similar X-ray reflection [12,22]. Raman spectroscopy is widely used to distinguish the three possible structures of ZrO_2 [23–25]. The Raman spectra of Yb/Tm: YSZ crystal chips are shown in Figure 2b. The Raman spectra of all samples are characterized by one strong peak in the wave-number range of

150–950 cm^{-1} . The Raman peak centered at around 625 cm^{-1} , corresponding to the F_{2g} mode of the cubic phase [26], is a little bigger than that of 0.5 Tm_2O_3 :YSZ single crystal [12], and it may be attributed to the presence of co-doped Yb_2O_3 . The diffraction patterns of all the samples match well with the standard card of cubic ZrO_2 (JCPDS No.97-008-9429), belonging to the $Fm\bar{3}m$ (225) space group. No extra peaks of a secondary phase were observed, indicating that Tm^{3+} and Yb^{3+} successfully entered the YSZ lattice. In addition, the cell parameters decrease slightly with the increase of Yb_2O_3 content, as seen in Table 2. This is due to the Yb^{3+} preferentially substituting for Y^{3+} , and the radius of Yb^{3+} (0.985 Å) is smaller than Y^{3+} (1.019 Å).

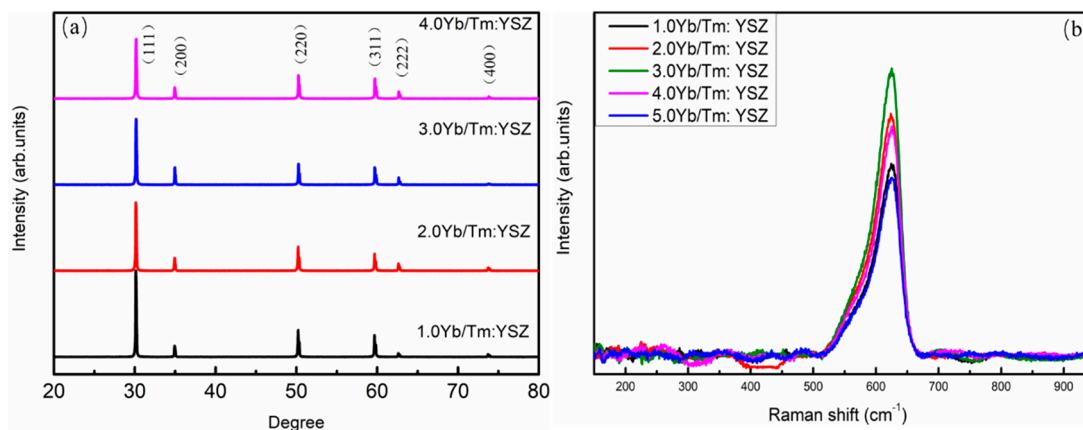


Figure 2. (a) XRD patterns for powders that were obtained by grinding x Yb/Tm:YSZ single crystals, (b) Raman spectra of x Yb/Tm:YSZ single crystals.

Table 2. Cell parameters of x Yb/Tm:YSZ single crystals.

Samples	Cell Parameters (Å)
	$a = b = c$
1.0Yb/Tm:YSZ	5.1590
2.0Yb/Tm:YSZ	5.1581
3.0Yb/Tm:YSZ	5.1580
4.0Yb/Tm:YSZ	5.1555

3.2. Absorption Spectra and Judd-Ofelt Analysis

The optical absorption spectra of x Yb/Tm:YSZ single crystals between 300 and 2000 nm were tested, as shown in Figure 3. There is no characteristic absorption related to $d-d$ transition in the range of 300–2000 nm because the d orbit of Zr^{4+} is empty. Therefore, the absorption peaks of all the samples are from the transitions between Tm^{3+} and Yb^{3+} . There are four visible and three IR absorption peaks, centering at 358, 460, 679, 783.5, 1200, and 1721.5 nm which correspond to the transitions of Tm^{3+} : $^3\text{H}_6 \rightarrow ^1\text{D}_2$, $^3\text{H}_6 \rightarrow ^1\text{G}_4$, $^3\text{H}_6 \rightarrow ^3\text{F}_{2,3}$, $^3\text{H}_6 \rightarrow ^3\text{H}_4$, $^3\text{H}_6 \rightarrow ^3\text{H}_5$, and $^3\text{H}_6 \rightarrow ^3\text{F}_4$, respectively. The strongest absorption peak is at around 850–1000 nm, corresponding to the transition of Yb^{3+} : $^2\text{F}_{7/2} \rightarrow ^2\text{F}_{5/2}$, which indicated that Yb^{3+} has a large absorption of the 980 nm laser excitation and is suitable as a sensitizer in the up-conversion luminescence of Tm^{3+} .

Optically, the Judd-Ofelt (J-O) theory, through an analysis of the oscillator strengths, the emission branching ratio and the radiative lifetime [27–29] is used for analyzing the possible transition mechanisms of the rare earth ions that are affected by the host materials.

Based on the absorption spectrum of 2.0Yb/Tm:YSZ single crystal chip, the oscillator strengths for an induced electric dipole transition from the initial state to the final state are calculated according to the Equation (1) [28,29].

$$f = \frac{8\pi^2 m c \sigma}{3h(2J+1)} \frac{(n^2+2)^2}{9n} \sum_{\lambda=2,4,6} \Omega_{\lambda} \langle 4f^N \Psi J // U^{\lambda} // 4f^N \Psi' J' \rangle^2 \quad (1)$$

where m , c , σ , h , J , and n are the electron mass, velocity of light, transition energy, Planck constant, total angular momentum, and index of refraction, respectively. Ω_{λ} ($\lambda = 2, 4$ and 6) is oscillator intensity parameter and U_{λ} ($\lambda = 2, 4$ and 6) is the reduced matrix element. The values of average wavelength and the measured and calculated oscillated strengths for the 2.0Yb/Tm: YSZ single crystal are collected in Table 3.

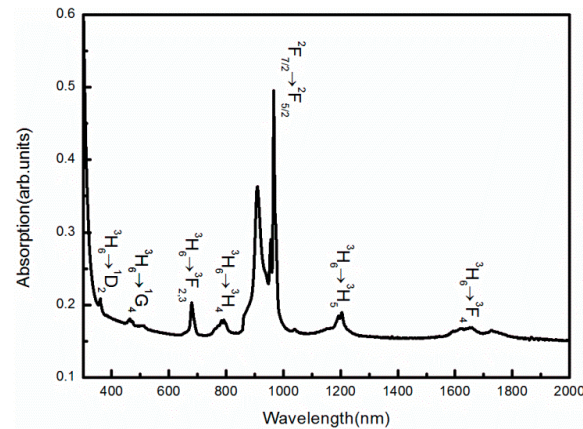


Figure 3. Absorption spectra of 2.0Yb/Tm: YSZ single crystal.

Table 3. Values of average wavelength and the experimental and calculated oscillated strengths for the 2.0Yb/Tm: YSZ single crystal.

3H_6	$\bar{\lambda}$ (nm)	Doubly Reduced Matrix Elements			Oscillator Strengths (10^{-20} cm^2)	
		$\ U^2\ ^2$	$\ U^2\ ^4$	$\ U^2\ ^6$	F_{exp}	F_{cal}
1D_2	359.62	0	0.3156	0.0928	0.0556	0.0533
1G_4	482.73	0.0483	0.0748	0.0125	0.0914	0.0309
${}^3F_2 + {}^3F_3$	679.96	0	0.3164	1.0922	0.2338	0.2093
3H_4	781.75	0.2373	0.1090	0.5947	0.1957	0.2028
3H_5	1193.25	0.1074	0.2314	0.6383	0.2802	0.1714
3F_4	1688.91	0.5375	0.7261	0.2382	0.3893	0.3465
RMS ΔS (10^{-20} cm^2)		0.077				

According to the J-O theory, the absorption oscillator strengths of Tm^{3+} ion are calculated, as shown in Table 3. The Judd–Ofelt parameters of Tm^{3+} in different host materials are listed in Table 4. The root mean square (RMS) is $0.077 \times 10^{-20} \text{ cm}^2$, indicating the high reliability of the obtained oscillator strengths. The intensity parameters Ω_{λ} ($\lambda = 2, 4, 6$) of Tm^{3+} are $0.41 \times 10^{-20} \text{ cm}^2$, $0.12 \times 10^{-20} \text{ cm}^2$, and $0.15 \times 10^{-20} \text{ cm}^2$. It is well known that the Ω_2 parameter is sensitive to crystal structure and related to the covalency of the RE^{3+} sites. While Ω_4 and Ω_6 depend on the viscosity and rigidity of the host material. The value of Ω_2 is larger than that of Ω_4 , revealing the relatively low symmetry of the Tm^{3+} site and the covalence that exists between the Tm^{3+} ions and anions as well as the asymmetry around the metal ion site [30]. According to the previous analysis, oxygen vacancies can be formed when the Y^{3+} , Tm^{3+} and Yb^{3+} ions occupy the sites of the small Zr^{4+} . Based on the theoretical calculation, the oxygen vacancies are located at the nearest neighbor of Zr^{4+} , leading to the seven-fold coordination and the symmetry reduction of the Zr^{4+} sites. It could be concluded that the Tm^{3+} occupy the Zr^{4+} site with seven coordination after entering YSZ lattice. Meanwhile, Ω_4/Ω_6 is one of the important parameters for the spectral characterization of the host materials. The value of Ω_4/Ω_6 for 2.0Yb/Tm: YSZ

single crystal is 0.8, which is larger than 0.68, 0.389, and 0.15 in LLF [31], YVO₄ [32], and SrWO₄ [33], revealing that the sample is a potential material for laser output.

Table 4. Judd–Ofelt parameters for Tm³⁺ doped in different hosts.

Crystal	Ω_2 (10 ^{−20} cm ²)	Ω_4 (10 ^{−20} cm ²)	Ω_6 (10 ^{−20} cm ²)	Ω_4/Ω_6	Ref
LLF	0.93	1.19	1.75	0.68	[31]
YVO ₄	9	1.05	2.7	0.389	[32]
SrWO ₄	7.41	0.25	0.98	0.15	[33]
YAG	0.7	1.2	0.5	2.4	[34]
YAP	0.67	2.30	0.74	3.108	[34]
YLF	2.42	1.28	0.90	1.422	[35]
SrGdGa ₃ O ₇	1.29	1.08	0.47	2.3	[36]
YSZ	0.41	0.12	0.15	0.80	This work

Using the Ω_λ values, the radiative properties such as spontaneous transition probability A_{ed} , branching ratios β , and radiative lifetime τ_{rad} for the transitions of Tm³⁺ in 2.0Yb/Tm: YSZ single crystal are calculated and listed in Table 5.

Table 5. Calculated radiative transition rates, branching ratios, and radiative lifetimes for different transition levels of 2.0Yb/Tm: YSZ single crystal.

Initial Level	Final Level	$\bar{\lambda}$ (nm)	A_{ed}	β	τ_{rad} (ms)
¹ G ₄	³ F ₂	1634	3.193	0.56	1.764
	³ F ₃	1494	14.006	2.47	
	³ H ₄	1177	59.520	10.50	
	³ F ₄	763	210.582	37.15	
	³ H ₅	666	42.751	7.54	
	³ H ₆	488	236.809	41.78	
³ H ₄	³ H ₅	2166	4.981	1.40	2.819
	³ F ₄	1432	27.057	7.63	
	³ H ₆	801.8	322.641	90.97	

3.3. Luminescence Properties

Figure 4 shows the emission spectra of the YSZ: 0.5 mol%Tm₂O₃, x mol%Yb₂O₃ (x = 1.0, 2.0, 3.0, 4.0, 5.0) in the wavelength range of 400–900 nm under the 980 nm laser excitation at room temperature. Clearly, under the excitation of 980 nm, the bright blue luminescence was observed by the naked eye, as shown in Figure 5. The emission spectra consisted of three main emission bands at around 488 (blue), 658 (red), and 799 nm (NIR), corresponding to the of ¹G₄→³H₆, ¹G₄→³F₄, and ³H₄→³H₆ transitions of Tm³⁺, respectively. Among these, the NIR emission corresponding to ³H₄→³H₆ at 799 nm is the dominant one, and is consistent with the literature. As the Yb₂O₃ concentration increases, the position and shape of the emission peaks is similar, indicating the same surrounding of Tm³⁺. In other words, the structure of YSZ crystals does not change significantly after Yb₂O₃ co-doping. The structure of the crystal affected the luminescence properties directly. The blue up-conversion luminescence of Tm³⁺ in cubic ZrO₂ is composed of three peaks, while it is a single peak in monoclinic ZrO₂. The blue emission band in Figure 4 is mainly composed of three peaks, indicating that the crystal structure is cubic, and it is consistent with the XRD and Raman spectroscopy results.

Figure 6 shows the intensities of the emission peaks of the samples. The luminescence intensity increases with an increase in Yb₂O₃ concentration up to 2.0 mol%, and then decreases dramatically, due to the concentration quenching effect. According to the Blasse theory, the process of non-radiative energy transfer depends on the radiative reabsorption or the electric multipolar interaction of the activated ion. However, the radiation reabsorption process only occurs in the case of a large overlap between the excitation spectrum of the sensitizer and the emission spectrum of the activator. As can be seen in Figure 4, the

emission peaks of Tm^{3+} are located at 488, 658, and 799 nm, while the absorption peak of the Yb^{3+} is located at around 980 nm, and the peak overlap is very small. Therefore, the concentration quenching in Yb/Tm: YSZ single crystals is induced by the electric multipolar interaction.

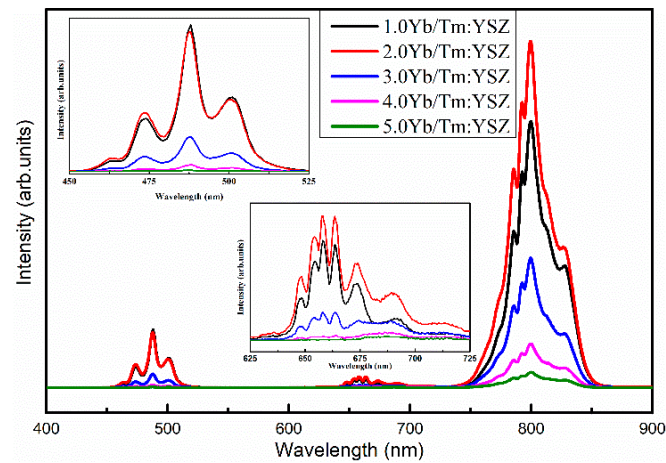


Figure 4. Up-conversion luminescence spectra for x Yb/Tm: YSZ crystals excited at 980 nm.

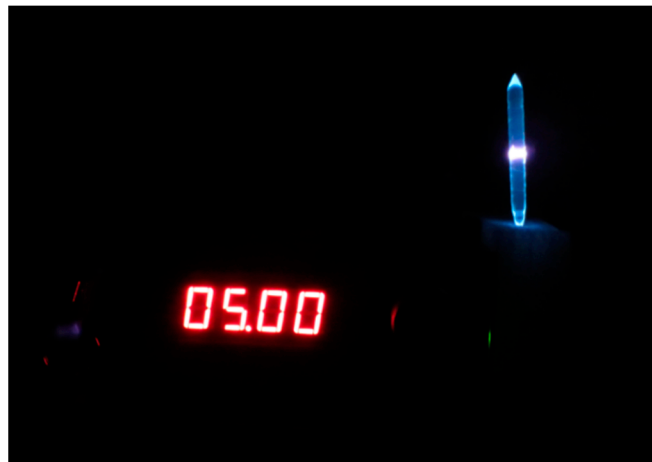


Figure 5. Photo of the 2.0Yb/Tm: YSZ single crystals under 980 nm laser excitation.

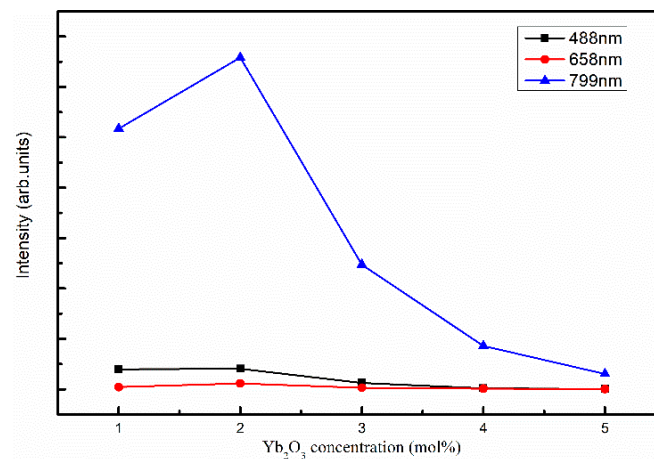


Figure 6. Intensities of emission peaks as a function of x in the x Yb/Tm: YSZ single crystal.

To examine the up-conversion mechanisms, the emission spectra of (0.5 mol%Tm₂O₃, 2.0 mol%Yb₂O₃): YSZ single crystal under 980 nm excitation at different power are plotted in Figure 7. The luminescence intensity (I) increases with the power (P), following the multiphoton formula, $I \propto P^n$. Here, n is the number of photons to populate the emitting states and is obtained by the slope of the linear fits of lg I–lg P curves. The slopes are 3.13, 3.30, and 2.32 for the blue emission centered at 488 nm, red emission centered at 658 nm, and NIR emission centered at 799 nm, respectively. This indicates that the red and blue emissions involve three photons while the NIR emission needs two photons. Although a photo avalanche (PA) is a possible mechanism for up-conversion luminescence, it is excluded because no inflection was observed in the power curve. Therefore, the up-conversion luminescence of Yb/Tm: YSZ single crystal is realized by the energy transfer (ET), the ground state absorption (GSA), and the excited state absorption (ESA) processes.

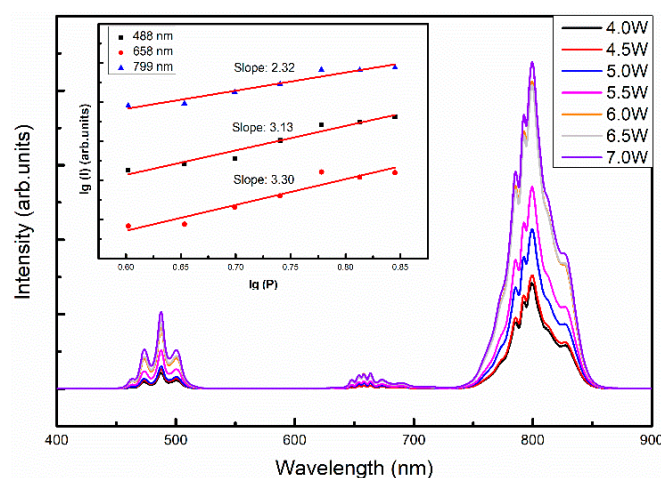


Figure 7. Up-conversion emission spectra of 2.0Yb/Tm: YSZ single crystal under the 980 nm excitation with different powers. The inset is the relationship between the up-conversion emission intensity and excitation power for the 2.0Yb/Tm: YSZ single crystal.

Figure 8 is the energy level diagram of the Yb³⁺-Tm³⁺ co-doped system. The transition processes in this up-conversion luminescence can be explained by the following. First, the electron of Yb³⁺ is excited from the ground state ²F_{7/2} to the ²F_{5/2} energy level by absorbing one 980 nm photon. Then, the Yb³⁺ transfers the energy to the ground state of neighboring Tm³⁺ according to the ET process. After that, the electron in the ³H₆ state of Tm³⁺ is excited to the ³H₅ state via the GSA process. The ³F₄ state is populated by the fast non-radiative relaxation. Following this, the Yb³⁺ absorbs the second photon and transfers the energy to the Tm³⁺, leading to the excitation of the electron from the ³F₄ state of Tm³⁺ to the ³F_{2,3} state via the ESA channel. Subsequently, the non-radiative transition between two activator ions will populate the ³H₄ state. Finally, the Yb³⁺ absorbs the third photon and transfers the energy to the ³H₄ state, leading to the electron excitation to the ¹G₄ state. Then, the up-conversion luminescence is generated by the transitions from the high to the low-energy states. Therefore, the emission of blue (488 nm), red (658 nm), and NIR (799 nm) are observed according to the ¹G₄→³H₆, ¹G₄→³F₄, and ³H₄→³H₆ transitions, respectively.

3.4. Luminescence Decay Kinetics

Figure 9a presents the fluorescence decay curve of the emission line ¹G₄→³F₄ (658 nm) of Tm³⁺ in x Yb/Tm: YSZ crystal (x = 1.0, 2.0, 3.0 mol%), excited by 980 nm at room temperature. From a single exponential function fitting, the average fluorescence lifetime τ of the ¹G₄→³F₄ transition of the x Yb/Tm: YSZ crystal (x = 1.0, 2.0, 3.0 mol%) is equal to 0.949 ms, 0.972 ms, and 0.953 ms, respectively. The 2.0Yb/Tm: YSZ single crystal has the longest lifetime. As the concentration of Tm³⁺ remains the same, the excited state lifetime of Tm³⁺ is affected by the energy transfer process between Yb³⁺ and Tm³⁺. In addition,

the fluorescence decay curve for Tm^{3+} for the ${}^1\text{G}_4 \rightarrow {}^3\text{H}_6$ (488 nm) transition in 2.0Yb/Tm: YSZ single crystal is shown in Figure 9b. The average fluorescence lifetime is 7.716 ms. The decay time is larger than that of Tm: LGYSO [37] (1.669 ms), Tm: YVO_4 [38] (1.9 ms), Tm: SSO [39] (1.14 ms), revealing the suitability of the YSZ crystal as a host material for luminescence of Tm^{3+} .

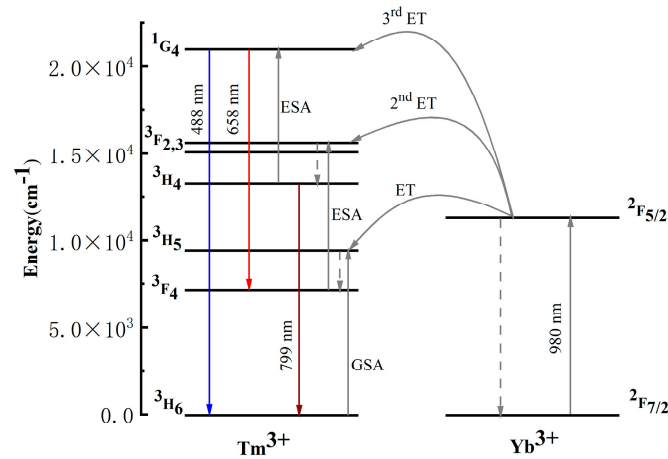


Figure 8. Energy level diagram of Tm^{3+} – Yb^{3+} energy transfer in the YSZ crystal under the 980 nm excitation. ET = energy transfer upconversion; GSA = ground state absorption; ESA = excited state absorption.

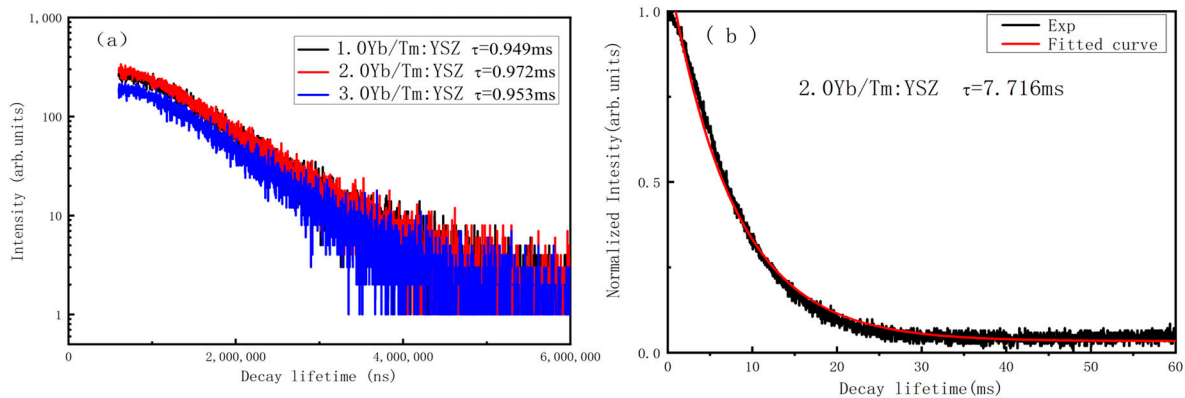


Figure 9. (a) Fluorescence decay curves for Tm^{3+} for ${}^1\text{G}_4 \rightarrow {}^3\text{F}_4$ (658nm) transition in Yb/Tm: YSZ single crystals; (b) Fluorescence decay curve for Tm^{3+} for ${}^1\text{G}_4 \rightarrow {}^3\text{H}_6$ (488 nm) transition in 2.0Yb/Tm: YSZ single crystal.

3.5. Color Chromaticity Coordinates

The color chromaticity characteristics of the Yb/Tm: YSZ single crystals were analyzed by the Commission International de l'éclairage (CIE) chromaticity coordinates diagram as shown in Figure 10 and Table 6. The color points of all the samples are in cyan region, and the purity of the blue emission is 79.5% for the 2.0Yb/Tm: YSZ single crystal.

Table 6. Values of CIE coordinates calculated for the various samples.

Sample	CIE x	CIE y
1.0Yb/Tm: YSZ	0.1080	0.2661
2.0Yb/Tm: YSZ	0.1164	0.2521
3.0Yb/Tm: YSZ	0.1116	0.2528
4.0Yb/Tm: YSZ	0.1057	0.2576

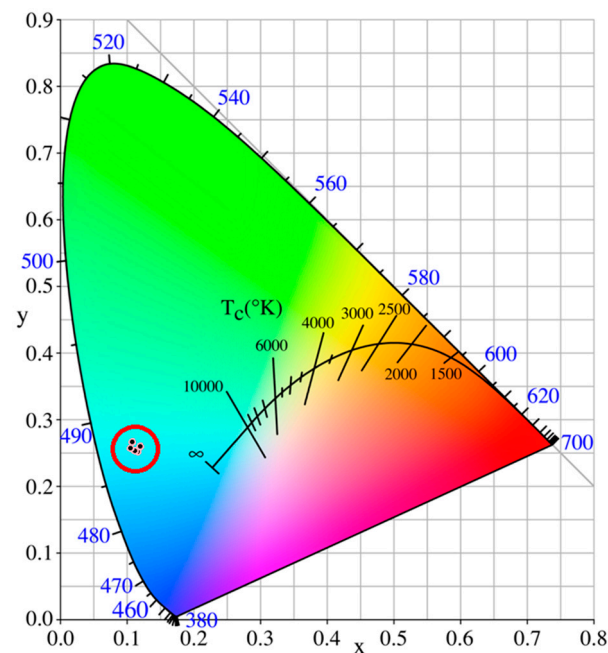


Figure 10. Chromaticity diagram for Yb/Tm: YSZ single crystals. All coordinates are in the red circle.

4. Conclusions

High-quality $\text{Yb}^{3+}/\text{Tm}^{3+}$ co-doped YSZ cubic single crystals were grown by the optical floating zone method. With an increasing concentration of Yb_2O_3 , the cell parameter decreases due to the Yb^{3+} preferential substitution for Y^{3+} . There were seven absorption peaks that were observed in the range of 300–2000 nm, corresponding to the transitions from $\text{Tm}^{3+} {}^3\text{H}_6$ ground state to the ${}^1\text{D}_2$ (358 nm), ${}^1\text{G}_4$ (460 nm), ${}^3\text{F}_{2,3}$ (679 nm), ${}^3\text{H}_4$ (783.3 nm), ${}^3\text{H}_5$ (1200 nm), and ${}^3\text{F}_4$ (1721.5 nm) excited states and that in the 850–1000 nm region of Yb^{3+} (${}^2\text{F}_{7/2} \rightarrow {}^2\text{F}_{5/2}$) transition. Based on the absorption spectrum, the oscillator strength parameters Ω_λ ($\lambda = 2, 4, 6$) were calculated by the Judd–Ofelt theory. The Ω_2 value is larger than Ω_4 , and it indicates that Tm^{3+} preferentially substituted for Zr^{4+} with seven coordination. There were three up-conversion emission peaks around 488, 658, and 799 nm that were observed when Yb/Tm: YSZ single crystal was excited with a 980 nm laser. The intensities of the emission peaks reached maximum when the concentration of Yb_2O_3 was 2.0 mol%, and then the concentration quenching effect appeared due to the electric multipole interaction. In addition, a two-photon process is involved for populating the ${}^3\text{H}_4$ level of Tm^{3+} , whereas a three-photon process is involved in the generation of blue emission. The energy transfer between Yb^{3+} and Tm^{3+} was confirmed by the changes of the lifetime of Tm^{3+} from the fluorescence decay, which also reached a maximum with 2.0 mol% Yb_2O_3 . The fluorescence lifetime of Tm^{3+} for ${}^1\text{G}_4 \rightarrow {}^3\text{H}_6$ transition was measured to be 7.716 ms for 2.0Yb/Tm: YSZ single crystal excited with a 980 nm laser. Furthermore, the color coordinates of the 2.0Yb/Tm: YSZ sample had a blue luminescence purity of 79.5%. Therefore, the 2.0Yb/Tm: YSZ single crystal is a potential candidate for the laser and luminescence applications.

Author Contributions: Conceptualization, D.H. and T.X.; methodology, B.F. and S.X.; software, Y.H.; validation, S.X., Y.H. and Z.Z.; formal analysis, W.D.; investigation, D.H.; resources, S.X. and W.D.; data curation, Y.H.; writing—original draft preparation, D.H.; writing—review and editing, Z.Z.; visualization, Y.H.; supervision, W.D.; project administration, S.X. and Y.H.; funding acquisition, S.X. and Y.H. All authors have read and agreed to the published version of the manuscript.

Funding: This work was financially supported by the Education Department of Guangxi Zhuang Autonomous Region, China under Grant No. 2021KY0017, the Chinese National Innovation Program of “Great Innovation Program” under Grant No. 202110593084, the Guangxi Natural Science Founda-

tion under Grant No. 2022GXNSFBA035447, and the National Natural Science Foundations of China under Grant No. 12105055 and 12265005.

Data Availability Statement: The data that were presented in this study are available on reasonable request from the corresponding author.

Acknowledgments: The authors gratefully thank Ding kang Xiong for useful discussions on the subject matter of this paper.

Conflicts of Interest: The authors declare no conflict of interest.

References

1. Yan, Z.; Xu, W.; Ying, Z.; Yan, L.; Xi, Y. Optical temperature sensing of up-conversion luminescence materials: Fundamentals and process. *J. Alloys Compd.* **2020**, *817*, 152691.
2. Naresh, V.; Adusumalli, V.; Park, Y.; Lee, N. NIR triggered NaYF₄:Yb³⁺,Tm³⁺@NaYF₄/CsPb(Br_{1-x}/I_x)₃ composite for up-converted white-light emission and dual-modal anti-counterfeiting applications. *Mater. Today Chem.* **2022**, *23*, 100752. [[CrossRef](#)]
3. Zhang, W.; Ji, X.; Chen, K.; Wang, C.; Sun, S. Thermochromic performance of a new temperature sensitive pigment based on rhodamine derivative in both liquid and solid systems. *Prog. Org. Coat.* **2019**, *137*, 105280. [[CrossRef](#)]
4. Peng, Z.; Wen, W.; Li, W.; Ya, W.; Sheng, T.; Ze, C.; Shou, X.; Bernard, G.; Wen, D. Up-conversion luminescence and Judd-Ofelt analysis of Nd₂O₃-doped yttria stabilized zirconia single crystals. *Crystengcomm* **2022**, *24*, 5977–5986.
5. Yong, Z.; Peng, L.; Xiang, L.; Hao, C.; Guo, X.; Zheng, Q. Up-conversion nanoparticles/PMMA composites for light-emitting applications. *Nano* **2021**, *15*, 2050023.
6. Xi, J.; Zhong, Z.; Tian, Z.; Ce, L.; Zhuang, L.; Wei, Y.; Xin, W.; Xue, S.; Xu, Z.; Hong, S.; et al. Enhanced up-conversion luminescence intensity of NaY(MoO₄)₂:Ho³⁺/Yb³⁺ phosphor by doping with Mg²⁺ ions for use in high-efficiency optical temperature sensor. *J. Lumines.* **2022**, *245*, 118759.
7. Qiu, H.; Qi, W.; Feng, H.; Zheng, X.; Lei, Z.; Su, Z. Multicolor coding up-conversion nanoplatfor for rapid screening of multiple foodborne pathogens. *ACS Appl. Mater. Interfaces* **2021**, *13*, 26782–26789.
8. Xiao, F.; Lai, G.; Yi, H.; Qi, Z. Uniform spheres of α-NaYF₄:RE³⁺ (RE = Eu, Tb, Ce, Er, and Tm): Template-free synthesis, multi-color photoluminescence, and their application in cellular imaging. *Crystals* **2020**, *10*, 119.
9. Xiang, L.; Yun, W.; Pan, Z.; Wan, G. Highly sensitivity, selectivity chemosensor for methyl orange using upconversion NaBiF₄:Yb/Tm nanosheets. *J. Solid State Chem.* **2021**, *301*, 122307.
10. Joshi, R.; Perala, R.; Shelar, S.; Ballal, A.; Singh, B.; Ning, R. Super Bright Red Upconversion in NaErF₄: 0.5%Tm @NaYF₄: 20%Yb Nanoparticles for Anti-counterfeit and Bioimaging Applications. *ACS Appl. Mater. Interfaces* **2021**, *13*, 3481–3490. [[CrossRef](#)] [[PubMed](#)]
11. Dai, W.; Wen, W.; Xiao, T.; Bernard, G.; Shou, X.; Wen, D. Upconversion visible light emission in Yb/Pr co-doped yttria-stabilized zirconia (YSZ) single crystals. *Crystals* **2021**, *11*, 1328.
12. Shou, X.; Xiao, T.; Fen, L.; Lei, Z.; Yu, H.; Bernard, G.; Wen, D. Growth and optical properties of thulia-doped cubic yttria stabilized zirconia single crystals. *Ceram. Int.* **2019**, *45*, 15974–15979.
13. Chang, L.; Aleksandr, A.; Maxim, M.; Aleksandr, A.; Victor, A. Microwave sol-gel synthesis and upconversion photoluminescence properties of CaGd₂(WO₄)₄:Er³⁺/Yb³⁺ phosphors with incommensurately modulated structure. *J. Solid State Chem.* **2015**, *228*, 160–166.
14. Sushil, R.; Manisha, M.; Vineet, R. Er³⁺-Yb³⁺/Er³⁺-Yb³⁺-Li⁺/Er³⁺-Yb³⁺-Zn²⁺:Gd₂O₃ nanophosphors for efficient frequency upconverter and temperature sensing applications. *Mater. Res. Bull.* **2018**, *106*, 66–73.
15. Chang, L.; Aleksandr, A.; Maxim, M.; Aleksandr, O.; Victor, A. Structural and spectroscopic effects of Li⁺ substitution for Na⁺ in Li_xNa_{1-x}CaGd_{0.5}Ho_{0.05}Yb_{0.45}(MoO₄)₃ scheelite-type upconversion phosphors. *Molecules* **2021**, *26*, 7357.
16. Krishna, K.; Upadhyay, M.; Kesarwani, V.; Kumar, K. Blue frequency upconversion emission and optical thermometry of Ca₃(PO₄)₂: Tm³⁺/Yb³⁺. *Optik* **2023**, *273*, 170477. [[CrossRef](#)]
17. Yan, W.; Mei, L.; Er, X.; Shou, X.; Yu, H.; Wen, D. Luminescent properties and first-principles calculations of (Cr,Ca):YAG crystals. *Int. J. Mod. Phys. B* **2017**, *31*, 1744070.
18. Wen, D.; Zhen, C.; Yan, M.; Xiu, C.; Ding, X.; Yu, H. Micro-defects and optical properties of YAG:Ce crystals prepared by optical floating zone method. *Int. J. Mod. Phys. B* **2017**, *31*, 1744068.
19. Xiu, C.; Xiao, L.; Xiao, C.; Shou, X.; Ding, X.; Wen, D. Preparation, characterization and optical properties of Dy-doped yttrium aluminum garnet. *Int. J. Mod. Phys. B* **2017**, *31*, 1744071.
20. Fen, L.; Xiao, T.; Shou, X.; Xiang, W.; Bernard, G.; Wen, D. Micro-defects and luminescence of thulium-doped yttrium aluminum garnet single crystals. *Physica B* **2022**, *628*, 413568.
21. Fen, L.; Bernard, G.; Xiao, T.; Xiang, W.; Dan, C.; Wen, D. Luminescence and EPR properties of high quality ruby crystals prepared by the optical floating zone method. *Opt. Mater.* **2019**, *91*, 183–188.
22. Li, S.; Long, Z.; Lei, L. Quantitative effect of Zr content on the structure and Water-Gas shift reaction activities of supported on Ceria-Zirconia. *Crystals* **2018**, *8*, 261.

23. Hua, C.; Xian, Q.; Bin, L.; Yu, L.; Yu, Z.; Rui, T.; Mei, Z.; Qi, Z. Synthesis and room-temperature ultraviolet photoluminescence properties of zirconia nanowires. *Adv. Funct. Mater.* **2004**, *14*, 243–246.
24. Soares, M.R.N.; Ferro, M.; Costa, F.M.; Monteiro, T. Upconversion luminescence and blackbody radiation in tetragonal YSZ co-doped with Tm^{3+} and Yb^{3+} . *Nanoscale* **2015**, *7*, 19958–19969. [[CrossRef](#)]
25. Xiao, T.; Shou, X.; Lei, Z.; Fen, L.; Bernard, G.; Wen, D. Preparation and optical properties of Ho^{3+} -doped YSZ single crystals. *Appl. Phys. A-Mater. Sci. Process.* **2018**, *124*, 853.
26. Yashima, M.; Ohtake, K.; Kakihana, M.; Arashi, H.; Yoshimura, M. Determination of tetragonal-cubic phase boundary of $\text{Zr}_{1-x}\text{R}_x\text{O}_{2-x/2}$ (R = Nd, Sm, Y, Er and Yb) by Raman scattering. *J. Phys. Chem. Solids* **1996**, *57*, 17–24. [[CrossRef](#)]
27. Jin, Z.; Zeng, X.; Xin, W.; Sheng, G.; Xin, L.; Fei, G. Ferroelectric and spectroscopic properties of $\text{Ho}^{3+}/\text{Yb}^{3+}$ co-doped $\text{Pb}(\text{Mg}_{1/3}\text{Nb}_{2/3})\text{O}_3\text{-}32\text{PbTiO}_3$ crystal. *Crystals* **2022**, *12*, 225.
28. Judd, B.R. Optical absorption intensities of rare-earth ions. *Phys. Rev.* **1962**, *127*, 750. [[CrossRef](#)]
29. Ofelt, G.S. Intensities of crystal spectra of rare-earth ions. *J. Chem. Phys.* **1962**, *37*, 511–520. [[CrossRef](#)]
30. Xiao, T.; Shou, X.; Fen, L.; Xiang, W.; Bernard, G.; Ding, X.; Wen, D. Highly efficient up-conversion green emission in Ho/Yb co-doped yttria-stabilized zirconia single crystals. *J. Lumines.* **2019**, *209*, 95–101.
31. Xiong, J.; Peng, H.; Zhao, C.; Huang, Y.; Zhang, L.; He, M.; Chen, G. Crystal growth, spectroscopic characterization, and laser performance of Tm: LiLuF_4 crystal. *Laser Phys. Lett.* **2009**, *6*, 868–871. [[CrossRef](#)]
32. Ermeueux, F.; Goutaudier, C.; Moncorge, R.; Cohen-Adad, M.; Bettinelli, M.; Cavalli, E. Growth and fluorescence properties of Tm^{3+} doped YVO_4 and Y_2O_3 single crystals. *Opt. Mater.* **1997**, *8*, 83–90. [[CrossRef](#)]
33. Caird, J.; DeShazer, L.; Nella, J. Characteristics of room-temperature 2.3- μm laser emission from Tm^{3+} in YAG and YAlO_3 . *IEEE J. Quantum Electron.* **1975**, *11*, 874–881. [[CrossRef](#)]
34. Weber, M.; Varitimos, T.; Matsinger, B. Optical intensities of rare-earth ions in yttrium orthoaluminate. *Phys. Rev. B.* **1973**, *8*, 47–53. [[CrossRef](#)]
35. Guo, J.; Chao, T.; Zhen, Y.; Jian, L.; Zhao, Z.; Bai, W. Thermal properties and polarized spectral analysis of Tm^{3+} : SrWO_4 crystal. *Solid State Commun.* **2005**, *134*, 583–588.
36. Gao, S.; Zhu, Z.; Wang, Y.; Li, J.; Tu, C. Polarized spectroscopic characterization and energy transfer of Tm^{3+} -, Ho^{3+} - $\text{BaLaGa}_3\text{O}_7$: New promising 2.0 μm laser crystals. *Laser Phys.* **2014**, *24*, 085004. [[CrossRef](#)]
37. Xing, H.; Rui, W.; Yi, W.; Pei, Z.; Si, Z.; Zhen, C.; Yi, Z.; Gui, Z. A novel crystal Tm: $\text{Lu}_{0.8}\text{Gd}_{0.8}\text{Y}_{0.4}\text{SiO}_5$ with potential for broadband tunable lasing. *Infrared Phys. Technol.* **2018**, *88*, 81–86.
38. Lisiecki, R.; Ryba-Romanowski, W.; Lukaszewicz, T. Relaxation of excited states of Tm^{3+} and Tm^{3+} - Eu^{3+} energy transfer in YVO_4 crystal. *Appl. Phys. B-Lasers Opt.* **2006**, *83*, 255–259. [[CrossRef](#)]
39. Kei, Y.; Tian, F.; Sheng, Z.; Cheng, L.; Tao, L.; Wei, M.; Zheng, Z.; Qing, W.; Liang, S.; Piotr, S.; et al. Spectral and laser performance of a Tm^{3+} : ScYSiO_5 crystal. *J. Alloys Compd.* **2017**, *712*, 412–417.

Disclaimer/Publisher's Note: The statements, opinions and data contained in all publications are solely those of the individual author(s) and contributor(s) and not of MDPI and/or the editor(s). MDPI and/or the editor(s) disclaim responsibility for any injury to people or property resulting from any ideas, methods, instructions or products referred to in the content.